

Nonrigid Registration Using Free-Form Deformations: Application to Breast MR Images

D. Rueckert,* L. I. Sonoda, C. Hayes, D. L. G. Hill, M. O. Leach, and D. J. Hawkes

Abstract— In this paper we present a new approach for the nonrigid registration of contrast-enhanced breast MRI. A hierarchical transformation model of the motion of the breast has been developed. The global motion of the breast is modeled by an affine transformation while the local breast motion is described by a free-form deformation (FFD) based on B-splines. Normalized mutual information is used as a voxel-based similarity measure which is insensitive to intensity changes as a result of the contrast enhancement. Registration is achieved by minimizing a cost function, which represents a combination of the cost associated with the smoothness of the transformation and the cost associated with the image similarity. The algorithm has been applied to the fully automated registration of three-dimensional (3-D) breast MRI in volunteers and patients. In particular, we have compared the results of the proposed nonrigid registration algorithm to those obtained using rigid and affine registration techniques. The results clearly indicate that the nonrigid registration algorithm is much better able to recover the motion and deformation of the breast than rigid or affine registration algorithms.

I. INTRODUCTION

CARCINOMA of the breast is the most common malignant disease in women in the western world. 9.5% of women will develop the disease in the United Kingdom [1]. The major goals of breast cancer diagnosis are early detection of malignancy and its differentiation from other breast disease. Currently, the detection and diagnosis of breast cancer primarily relies on X-ray mammography. For further differentiation of mammographic or clinical abnormalities, ultrasonography, transcutaneous biopsy, and MRI are used. Although X-ray mammography has the advantage of high sensitivity, almost approaching 100%, in fatty breast tissue, high resolution up to 50 μm , and low cost, it has a number of disadvantages, such as low sensitivity in dense glandular breast tissue, low specificity, and poor signal-to-noise ratio. Furthermore, the projective nature of the images and the exposure to radiation limit its applicability, especially for

young premenopausal women with a genetic predisposition to develop breast cancer.

This has led to the investigation of alternative imaging modalities, such as MRI, for the detection and diagnosis of breast cancer [2]. Even though MRI mammography has disadvantages, such as a low spatial resolution of around 1 mm and the need for contrast agents, it has a number of advantages, including the tomographic, and therefore three-dimensional (3-D) nature, of the images. This allows the application of MRI mammography to breasts with dense tissue, postoperative scarring, and silicon implants. Furthermore, the lack of radiation makes it applicable to young premenopausal women. Typically, the detection of breast cancer in MRI requires the injection of a contrast agent such as Gadolinium DTPA. It is known that the contrast agent uptake curves of malignant disease differ from benign disease and this property can be used to identify cancerous lesions [3]. To quantify the rate of uptake, a 3-D MRI scan is acquired prior to the injection of contrast media, followed by a dynamic sequence of 3-D MRI scans. The rate of uptake can be estimated from the difference between pre- and postcontrast images. Any motion of the patient between scans, or even normal respiratory and cardiac motion, complicates the estimation of the rate of uptake of contrast agent by the breast tissue.

To facilitate the analysis of pre- and postcontrast enhanced MRI, Zuo *et al.* [4] proposed a registration algorithm which minimizes the ratio of variance between images. However, their algorithm is based on the assumption that the breast is only undergoing rigid motion. Kumar *et al.* [5] proposed a nonrigid registration technique which uses an optical-flow type algorithm, but is based on the assumption that the intensities in the pre- and postcontrast enhanced images remain constant. A similar approach has been suggested by Fischer *et al.* [6]. To overcome the problems caused by nonuniform intensity change, Hayton *et al.* [7] developed a pharmacokinetic model, which is combined with an optical-flow registration algorithm. This algorithm has been applied to the registration of two-dimensional (2-D) breast MRI, but relies on the assumption that the change of intensities can be sufficiently explained by the pharmacokinetic model, which is not always the case.

Any registration algorithm for the motion correction of contrast-enhanced breast MRI must take into account that the breast tissue deforms in a nonrigid fashion and that the image intensity and contrast will change, due to the uptake of the contrast agent. In recent years, many voxel-based similarity measures have shown promising results for multimodality image registration (for a detailed overview see

Manuscript received November 4, 1998; revised July 6, 1998. the work of D. Rueckert and D. J. Hawkes was supported by in part by the EPSRC Project under Grant GR/L08519. The work C. Hayes and M. O. Leach was supported in part by the MRC under Grant G9600413 and in part by the CRC under Grant SP1780/0103. The Associate Editor responsible for coordinating the review of this paper and recommending its publication was D. Metaxas. Asterisk indicates corresponding author.

*D. Rueckert, L. I. Sonoda, D. L. G. Hill, and D. J. Hawkes are with the Division of Radiological Sciences and Medical Engineering, Guy's, King's, and St. Thomas' School of Medicine, King's College London, Guy's Hospital, London SE1 9RT, U.K. (e-mail: D.Rueckert@umds.ac.uk).

C. Hayes and M. O. Leach are with the CRC Clinical Magnetic Resonance Research Group, Institute of Cancer Research, Royal Marsden Hospital, Sutton SM2 5PT, U.K.

Publisher Item Identifier S 0278-0062(99)08508-0.

[8]). In particular, voxel-based similarity measures based on joint entropy [9], mutual information [10]–[13], and normalized mutual information [14], [15] have been shown to align images acquired with different imaging modalities, robustly. However, most of these approaches are limited either to rigid or affine transformations. In contrast, many nonrigid registration algorithms based on elastic deformations, such as animal [16] or demons [17], rely on the assumption that the intensity of tissues between images remains constant. This is also true for nonrigid registration algorithms based on fluid deformations [18], [19]. A notable exception is the registration algorithm proposed by Meyer *et al.* [20], which is based on a thin-plate spline deformation and uses mutual information as a voxel-based similarity measure. However, due to prohibitive computational complexity of the thin-plate spline warps, the registration is restricted to a very limited number of degrees of freedom. This is not sufficient for most applications, which involve significant nonrigid deformations.

In this paper, we develop an algorithm for the nonrigid registration of 3-D contrast-enhanced breast MRI, which combines the advantages of voxel-based similarity measures, such as mutual information, with a nonrigid transformation model of the breast. The next section introduces a hierarchical transformation model which captures the global and local motion of the breast. The global motion of the breast is modeled by an affine transformation, while the local breast motion is described by a free-form deformation (FFD) based on B-splines. Since the intensity and contrast between the pre- and postcontrast enhanced images will change, we will use voxel-based similarity measures based on normalized mutual information. Section III shows results of the application of the algorithm to volunteer as well as clinical patient data. In addition, the results obtained by the nonrigid registration algorithm are compared with those of rigid and affine registration algorithms. These results demonstrate that rigid and affine transformation models often are not sufficient to model the motion of the breast adequately. Finally, Section IV summarizes the results and discusses current and future work in this area.

II. IMAGE REGISTRATION

The goal of image registration in contrast-enhanced breast MRI is to relate any point in the postcontrast enhanced sequence to the precontrast enhanced reference image, i.e., to find the optimal transformation $\mathbf{T}: (x, y, z) \mapsto (x', y', z')$ which maps any point in the dynamic image sequence $I(x, y, z, t)$ at time t into its corresponding point in the reference image $I(x', y', z', t_0)$, taken at time t_0 . In general, the motion of the breast is nonrigid so that rigid or affine transformations alone are not sufficient for the motion correction of breast MRI. Therefore, we develop a combined transformation \mathbf{T} which consists of a global transformation and a local transformation

$$\mathbf{T}(x, y, z) = \mathbf{T}_{\text{global}}(x, y, z) + \mathbf{T}_{\text{local}}(x, y, z). \quad (1)$$

A. Global Motion Model

The global motion model describes the overall motion of the breast. The simplest choice is a rigid transformation which is parameterized by 6 degrees of freedom, describing the rotations and translations of the breast. A more general class of transformations are affine transformations, which have six additional degrees of freedom, describing scaling and shearing. In 3-D, an affine transformation can be written as

$$\mathbf{T}_{\text{global}}(x, y, z) = \begin{pmatrix} \theta_{11} & \theta_{12} & \theta_{13} \\ \theta_{21} & \theta_{22} & \theta_{23} \\ \theta_{31} & \theta_{32} & \theta_{33} \end{pmatrix} \begin{pmatrix} x \\ y \\ z \end{pmatrix} + \begin{pmatrix} \theta_{14} \\ \theta_{24} \\ \theta_{34} \end{pmatrix} \quad (2)$$

where the coefficients Θ parameterize the 12 degrees of freedom of the transformation. In a similar fashion, the global motion model can be extended to higher order global transformations, such as trilinear or quadratic transformations [21].

B. Local Motion Model

The affine transformation captures only the global motion of the breast. An additional transformation is required, which models the local deformation of the breast. The nature of the local deformation of the breast can vary significantly across patients and with age. Therefore, it is difficult to describe the local deformation via parameterized transformations. Instead, we have chosen an FFD model, based on B-splines [22], [23], which is a powerful tool for modeling 3-D deformable objects and has been previously applied to the tracking and motion analysis in cardiac images [24]. The basic idea of FFD's is to deform an object by manipulating an underlying mesh of control points. The resulting deformation controls the shape of the 3-D object and produces a smooth and C^2 continuous transformation.

To define a spline-based FFD, we denote the domain of the image volume as $\Omega = \{(x, y, z) | 0 \leq x < X, 0 \leq y < Y, 0 \leq z < Z\}$. Let Φ denote a $n_x \times n_y \times n_z$ mesh of control points $\phi_{i,j,k}$ with uniform spacing δ . Then, the FFD can be written as the 3-D tensor product of the familiar 1-D cubic B-splines

$$\begin{aligned} \mathbf{T}_{\text{local}}(x, y, z) \\ = \sum_{l=0}^3 \sum_{m=0}^3 \sum_{n=0}^3 B_l(u) B_m(v) B_n(w) \phi_{i+l, j+m, k+n} \end{aligned} \quad (3)$$

where $i = \lfloor x/n_x \rfloor - 1$, $j = \lfloor y/n_y \rfloor - 1$, $k = \lfloor z/n_z \rfloor - 1$, $u = x/n_x - \lfloor x/n_x \rfloor$, $v = y/n_y - \lfloor y/n_y \rfloor$, $w = z/n_z - \lfloor z/n_z \rfloor$ and where B_l represents the l th basis function of the B-spline [22], [23]

$$\begin{aligned} B_0(u) &= (1-u)^3/6 \\ B_1(u) &= (3u^3 - 6u^2 + 4)/6 \\ B_2(u) &= (-3u^3 + 3u^2 + 3u + 1)/6 \\ B_3(u) &= u^3/6. \end{aligned}$$

In contrast to thin-plate splines [25] or elastic-body splines [26], B-splines are locally controlled, which makes them computationally efficient even for a large number of control points. In particular, the basis functions of cubic B-splines

have a limited support, i.e., changing control point $\phi_{i,j,k}$ affects the transformation only in the local neighborhood of that control point.

The control points Φ act as parameters of the B-spline FFD and the degree of nonrigid deformation which can be modeled depends essentially on the resolution of the mesh of control points Φ . A large spacing of control points allows modeling of global nonrigid deformations, while a small spacing of control points allows modeling of highly local nonrigid deformations. At the same time, the resolution of the control point mesh defines the number of degrees of freedom and, consequently, the computational complexity. For example, a B-spline FFD defined by a $10 \times 10 \times 10$ mesh of control points yields a transformation with 3000 degrees of freedom. The tradeoff between model flexibility and computational complexity is mainly an empirical choice which is determined by the accuracy required to model the deformability of the breast tissue versus the increase in computing time. In order to achieve the best compromise between the degree of nonrigid deformation required to model the motion of the breast and the associated computational cost, we have implemented a hierarchical multiresolution approach [23] in which the resolution of the control mesh is increased, along with the image resolution, in a coarse to fine fashion.

Let Φ^1, \dots, Φ^L denote a hierarchy of control point meshes at different resolutions. For simplicity, we will assume that the spacing between control points decreases from Φ^l to control mesh Φ^{l+1} , i.e., the resolution of the control mesh is increasing. Each control mesh Φ^l and the associated spline-based FFD defines a local transformation $\mathbf{T}_{\text{local}}^l$ at each level of resolution and their sum defines the local transformation $\mathbf{T}_{\text{local}}$

$$\mathbf{T}_{\text{local}}(x, y, z) = \sum_{l=1}^L \mathbf{T}_{\text{local}}^l(x, y, z). \quad (4)$$

In this case, the local transformation is represented as a combination of B-spline FFD's at increasing resolutions of the control point mesh. To avoid the overhead of calculating several B-spline FFD's separately, we represent the local transformation by a single B-spline FFD whose control point mesh is progressively refined. In this case, the control point mesh at level l is refined by inserting new control points to create the control point mesh at level $l+1$. We will assume that the control point spacing is halved in every step. In this case, the position of control point $\phi_{2i,2j,2k}^{l+1}$ coincides with that of control point $\phi_{i,j,k}^l$ and the values of the new control points Φ^{l+1} can be calculated directly from those of Φ^l , using a B-spline subdivision algorithm [27].

In general, the local deformation of the breast tissues should be characterized by a smooth transformation. To constrain the spline-based FFD transformation to be smooth, one can introduce a penalty term which regularizes the transformation. The general form of such a penalty term has been described by Wahba [28]. In 3-D, the penalty term takes the following form:

$$\mathcal{C}_{\text{smooth}} = \frac{1}{V} \int_0^X \int_0^Y \int_0^Z \left[\left(\frac{\partial^2 \mathbf{T}}{\partial x^2} \right)^2 + \left(\frac{\partial^2 \mathbf{T}}{\partial y^2} \right)^2 \right. \\ \left. + \left(\frac{\partial^2 \mathbf{T}}{\partial z^2} \right)^2 + 2 \left(\frac{\partial^2 \mathbf{T}}{\partial xy} \right)^2 + 2 \left(\frac{\partial^2 \mathbf{T}}{\partial xz} \right)^2 + 2 \left(\frac{\partial^2 \mathbf{T}}{\partial yz} \right)^2 \right] dx dy dz \quad (5)$$

where V denotes the volume of the image domain. This quantity is the 3-D counterpart of the 2-D bending energy of a thin-plate of metal and defines a cost function which is associated with the smoothness of the transformation. Note that the regularization term is zero for any affine transformations and, therefore, penalizes only nonaffine transformations [28].

C. Normalized Mutual Information

To relate a postcontrast enhanced image to the precontrast enhanced reference image, we must define a similarity criterion which measures the degree of alignment between both images. Given that the image intensity might change after the injection of the contrast agent, one cannot use a direct comparison of image intensities, i.e., sum of squared differences or correlation, as a similarity measure. An alternative voxel-based similarity measure is mutual information (MI), which has been independently proposed by Collignon [10] and Viola [11], and which has been shown to align images from different modalities accurately and robustly [29]. Mutual information is based on the concept of information theory and expresses the amount of information that one image A contains about a second image B

$$\mathcal{C}_{\text{similarity}}(A, B) = H(A) + H(B) - H(A, B) \quad (6)$$

where $H(A)$, $H(B)$ denote the marginal entropies of A , B and $H(A, B)$ denotes their joint entropy, which is calculated from the joint histogram of A and B . If both images are aligned, the mutual information is maximized. It has been shown by Studholme [14] that mutual information itself is not independent of the overlap between two images. To avoid any dependency on the amount of image overlap, Studholme suggested the use of normalized mutual information (NMI) as a measure of image alignment

$$\mathcal{C}_{\text{similarity}}(A, B) = \frac{H(A) + H(B)}{H(A, B)}. \quad (7)$$

Similar forms of normalized mutual information have been proposed by Maes *et al.* [15].

D. Optimization

To find the optimal transformation, we minimize a cost function associated with the global transformation parameters Θ , as well as the local transformation parameters Φ . The cost function comprises two competing goals. The first term represents the cost associated with the image similarity $\mathcal{C}_{\text{similarity}}$ in (7), while the second term corresponds to the cost associated with the smoothness of the transformation $\mathcal{C}_{\text{smooth}}$ in (5)

$$\mathcal{C}(\Theta, \Phi) = -\mathcal{C}_{\text{similarity}}(I(t_0), \mathbf{T}(I(t))) + \lambda \mathcal{C}_{\text{smooth}}(\mathbf{T}). \quad (8)$$

Here, λ is the weighting parameter which defines the tradeoff between the alignment of the two image volumes and the

calculate the optimal affine transformation parameters Θ by maximising eq. (7)

initialize the control points Φ .

repeat

calculate the gradient vector of the cost function in eq. (8) with respect to the non-rigid transformation parameters Φ :

$$\nabla \mathcal{C} = \frac{\partial \mathcal{C}(\Theta, \Phi^l)}{\partial \Phi^l}$$

while $\|\nabla \mathcal{C}\| > \epsilon$ **do**

recalculate the control points $\Phi = \Phi + \mu \frac{\nabla \mathcal{C}}{\|\nabla \mathcal{C}\|}$

recalculate the gradient vector $\nabla \mathcal{C}$

increase the control point resolution by calculating new control points Φ^{l+1} from Φ^l .

increase the image resolution.

until finest level of resolution is reached.

Fig. 1. The nonrigid registration algorithm.

smoothness of the transformation. For the purpose of this paper, we have determined the value of λ experimentally and found that a value of $\lambda = 0.01$ provides a good compromise between the two competing terms of the cost function. We have also observed that the intrinsic smoothness properties of B-splines mean that the choice of λ is not critical for low resolutions of the control point mesh. The regularization term is more important for high resolutions of the control point mesh. The reason for this is the fact that the ability of the FFD to model localized deformations increases with decreasing control point spacing. This raises the need for regularization, especially for dense control point meshes.

For computational efficiency, the optimization proceeds in several stages. During the first stage, the affine transformation parameters Θ are optimized, using an iterative multiresolution search strategy [13]. Since the smoothness term of the cost function in (5) is zero for any affine transformation, this step is equivalent to maximizing the image similarity measure defined in (7). During the subsequent stage, the nonrigid transformation parameters Φ are optimized as a function of the cost function in (8). In each stage, we employ a simple iterative gradient descent technique which steps in the direction of the gradient vector with a certain step size μ . The algorithm stops if a local optimum of the cost function has been found. In practice, it is sufficient to assume a local optimum if $\|\nabla \mathcal{C}\| \leq \epsilon$ for some small positive value ϵ . The nonrigid registration algorithm can be summarized in Fig. 1.

III. RESULTS

We have applied the registration algorithm to volunteer data without contrast enhancement, as well as to clinical patient data with contrast enhancement. To assess the quality of the registration in volunteer data, we have calculated the mean and variance of the squared sum of intensity differences (SSD)

$$\text{SSD} = \frac{1}{n} \sqrt{\sum (I(t_0) - \mathbf{T}(I(t)))^2} \quad (9)$$

as well as the correlation coefficient (CC)

$$\text{CC} = \frac{\sum (I(t_0) - \bar{I}(t_0))(\mathbf{T}(I(t)) - \mathbf{T}(\bar{I}(t)))}{\sqrt{\sum (I(t_0) - \bar{I}(t_0))^2 \sum (\mathbf{T}(I(t)) - \mathbf{T}(\bar{I}(t)))^2}}. \quad (10)$$

Here $\bar{I}(t_0)$, $\bar{I}(t)$ denote the average intensities of the images before and after motion and the summation includes all voxels within the overlap of both images. In these images, the SSD and the CC provide an indirect measure of the registration quality as the position of the breast tissue changes, but the tissue composition, and hence image intensity, does not. Since the motion of each breast is normally uncorrelated, we have manually defined a rectangular region of interest (ROI) around each breast and then registered both ROI's independently.

A. Volunteer Data

To test the ability of the algorithm to correct the nonrigid motion of the breast, two separate 3-D MR scans of eight volunteers were acquired (aged between 28–47 yr). After the first scan each volunteer was asked to move inside the scanner. For the volunteer studies, a 3-D FLASH sequence was used with TR = 12 ms, TE = 5 ms, flip angle = 35°, FOV = 340 mm, and coronal slice orientation. The MR images were acquired on a 1.5 Tesla Siemens Vision MR system without contrast enhancement. The images have a size of 256 × 256 × 64 voxels and spatial resolution of 1.33 × 1.33 × 2.5 mm. An example of these images before and after motion is shown in Fig. 2(a) and (b). The corresponding difference image is shown in Fig. 2(c). Ideally, we would expect that the difference image only shows the underlying noise of the image acquisition. However, the effect of the misregistration due to the motion of the breast is clearly visible in the difference image. We have compared three different types of transformations: Pure rigid and affine transformations as well as the proposed nonrigid transformation model. The registration results based on the different transformation models and the corresponding difference images are shown in Fig. 3(a)–(f). After rigid and affine registration there is

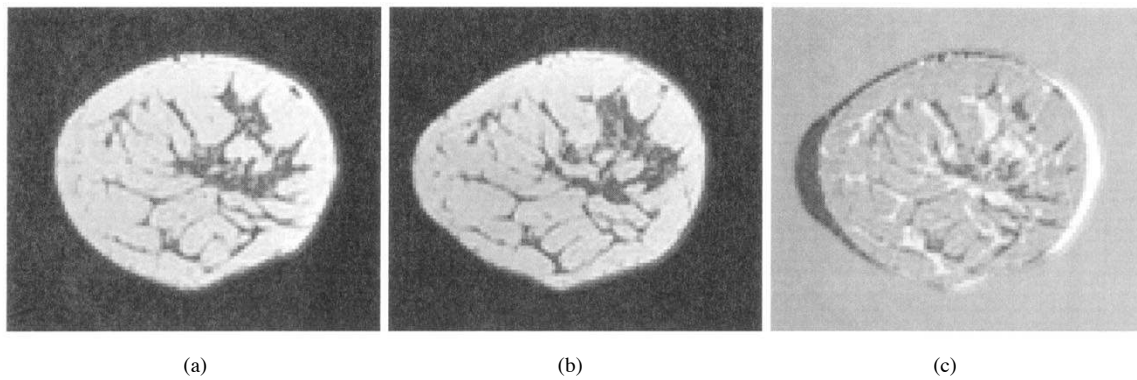


Fig. 2. Example of misregistration caused by motion of a volunteer. (a) Before motion. (b) After motion. (c) After subtracting (b) from (a) without registration.

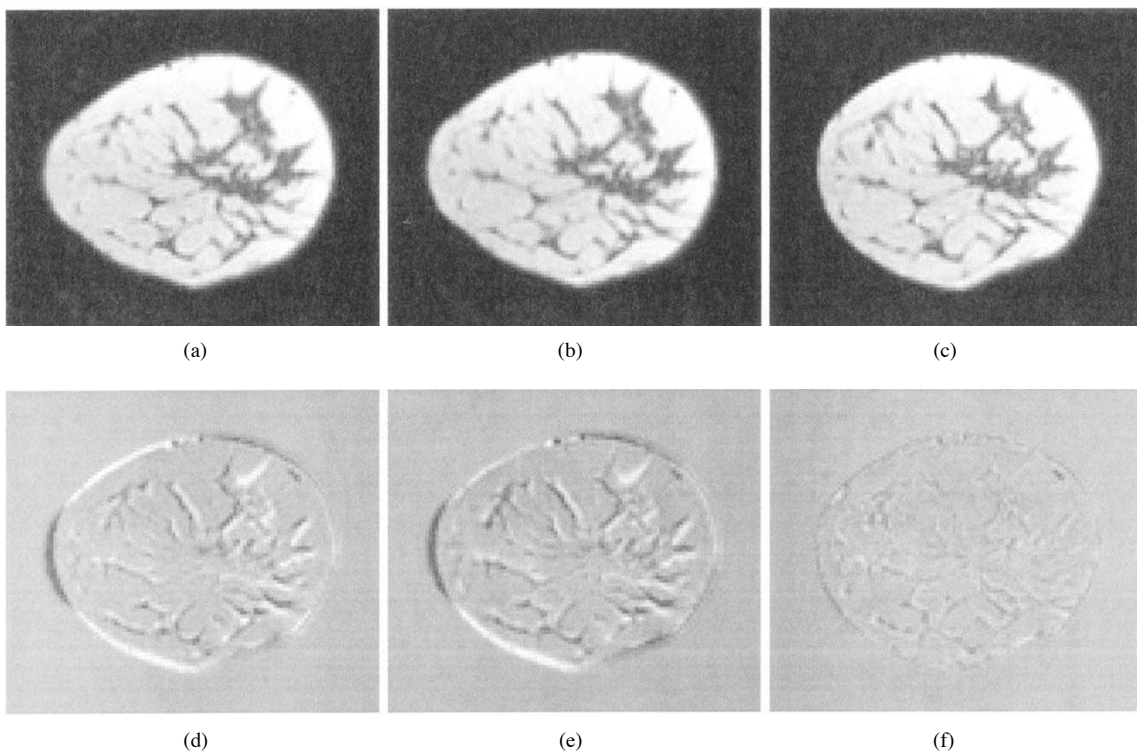


Fig. 3. Example of different transformations on the registration for the volunteer study in Fig. 2: after (a) rigid, (b) affine, and (c) nonrigid registration. The corresponding difference images are shown in (d)–(f).

still a considerable amount of misregistration visible in the difference image. However, after nonrigid registration the amount of misregistration visible in the difference image has been reduced significantly.

Table I summarizes the results of the registration quality of the volunteer datasets in terms of squared sum of intensity differences (SSD) and correlation coefficient (CC) for the different transformation models. The results clearly show that the registrations which are based on rigid or affine transformations improve the correlation between the images before and after motion. However, both transformation models perform significantly worse than the proposed nonrigid transformation model. The results also show that the nonrigid registration performs better as the resolution of the control point mesh of the spline-based FFD increases. While a control point spacing of 20 mm yields already improved correlation compared to

affine transformations, a control point spacing of 15 or 10 mm yields even higher correlation. The main reason for this is the increased flexibility of the spline-based FFD to describe local deformations of the breast as the number of control points increases.

In addition we performed a second experiment in which we wanted to assess the ability of the algorithm to correct for different degrees of motion. The imaging protocol consists of six consecutive 3-D MR scans of two volunteers, using the same image acquisition parameters as described earlier. Between each scan the volunteers were asked to move by a different amount. The amount of motion the volunteers were asked to simulate was: 1) no movement, 2) cough, 3) move head, 4) move arm, and 5) lift out of coil and back. As before, we compared rigid, affine, and nonrigid registration with no registration. The results are summarized in Figs. 4 and 5.

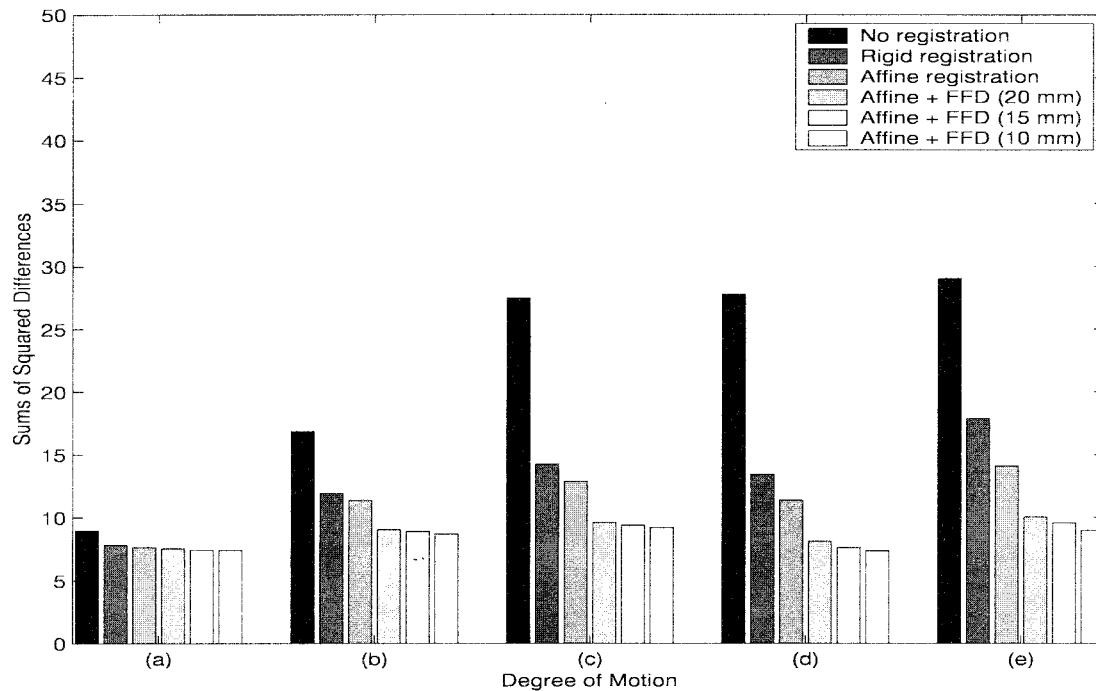


Fig. 4. Comparison of the registration error in terms of SSD for different degrees of volunteer motion. (a) No voluntary movement. (b) Cough. (c) Move head. (d) Move arm. (e) Lift out of coil and back.

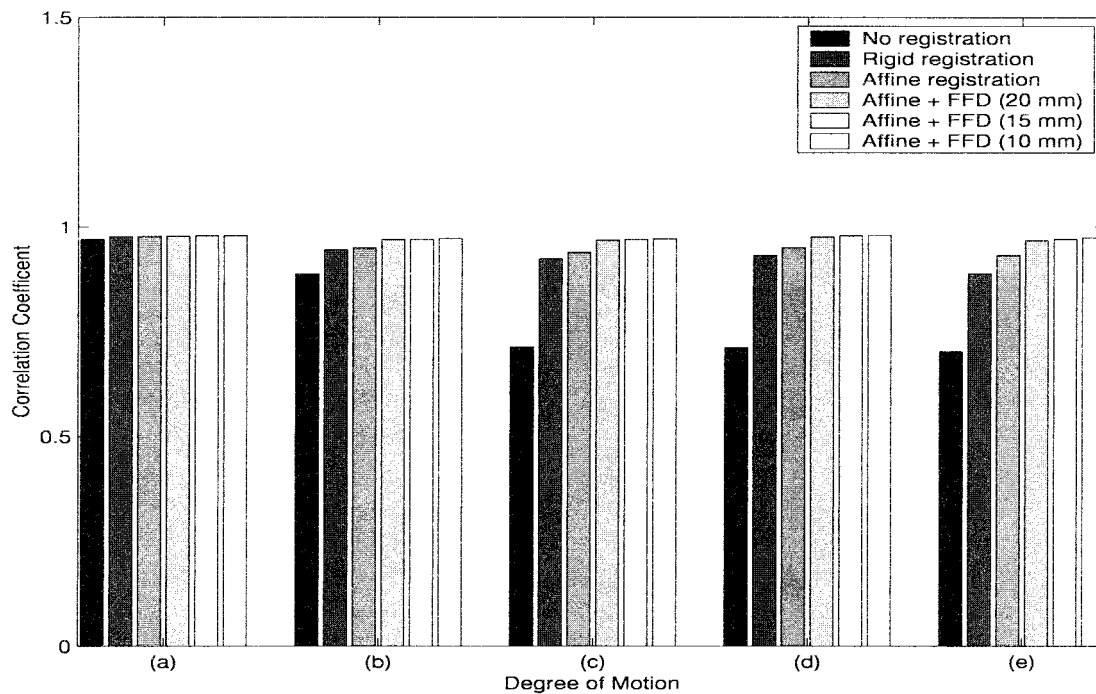


Fig. 5. Comparison of the registration error in terms of CC for different degrees of volunteer motion. (a) No voluntary movement. (b) Cough. (c) Move head. (d) Move arm. (e) Lift out of coil and back.

Fig. 4 compares the registration error in terms of SSD for the different degrees motion: In the case of no movement, all registration techniques provide a very similar improvement, compared to no registration. However, in all other cases the nonrigid registration performs better than rigid or affine registration. Furthermore, the nonrigid registration performs better at a control point spacing of 10 mm than at 20 or

15 mm. A similar observation can be made by comparing the correlation coefficient (CC) in Fig. 5 between the images with and without registration.

B. Patient Data

We have also applied the algorithm to contrast-enhanced MR images from a group of eight different patients. For the

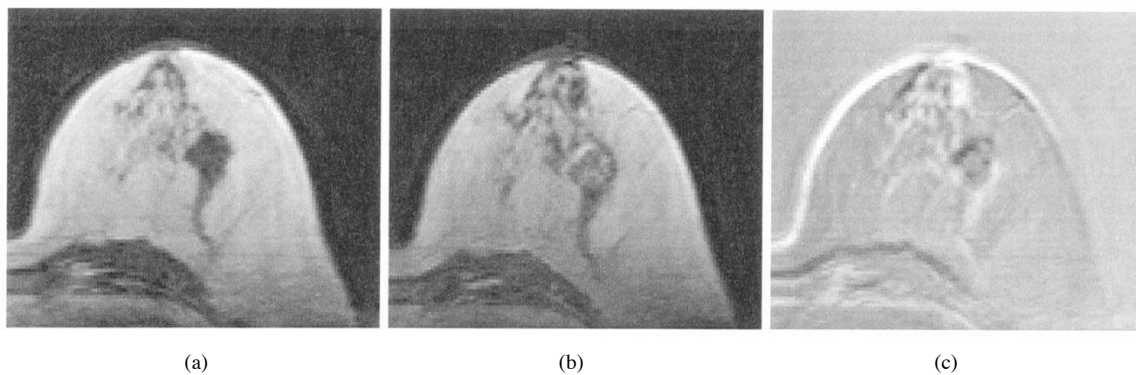


Fig. 6. Example of misregistration in a contrast-enhanced patient study. (a) Before injection of the contrast medium. (b) After injection of the contrast medium. (c) After subtraction of (a) and (b) without registration.

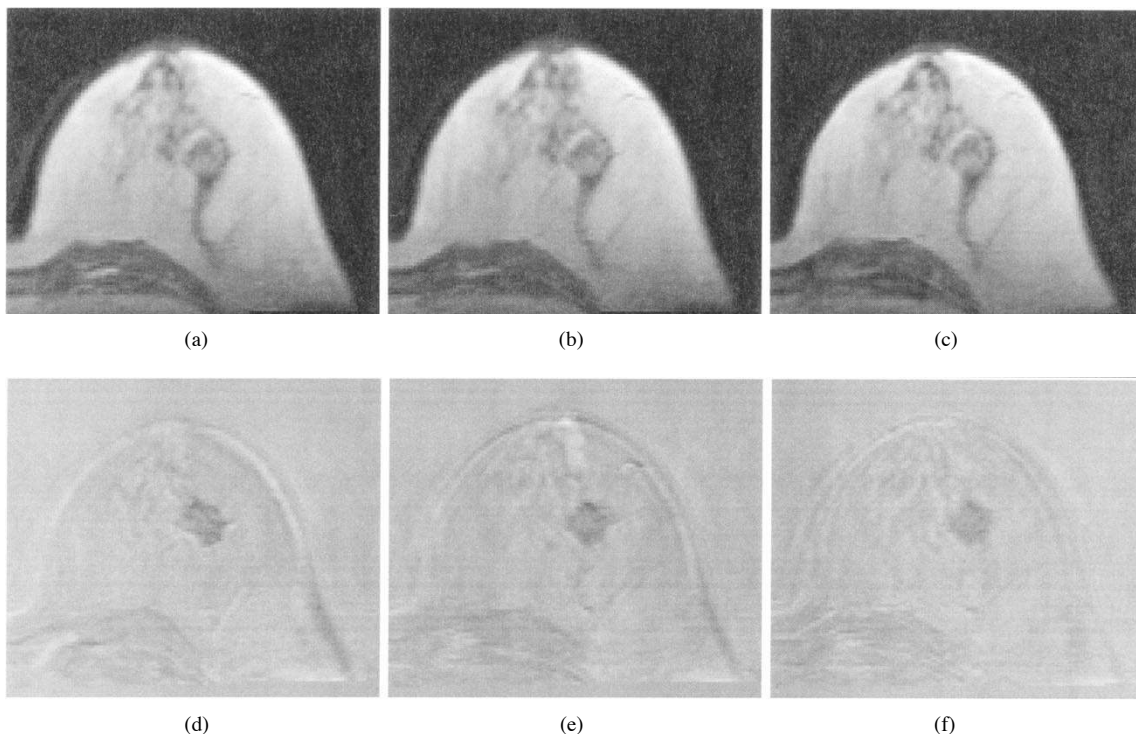


Fig. 7. Example of different transformations on the registration for the patient study in Fig. 6. (a) After rigid. (b) After affine. (c) After nonrigid registration. The corresponding difference images are shown in (d)–(f).

patient studies, a sequence of six 3-D scans was used with $TR = 12$ ms, $TE = 5$ ms, flip angle $= 35^\circ$, $FOV = 350$ mm, and axial slice orientation. The MR images were acquired on a 1.5-T Siemens Vision MR system with Gd-DTPA (Magnevist, Schering) contrast enhancement. The images have a size of 256×256 voxels and a spatial resolution of $1.37 \times 1.37 \times 4.2$ mm. A typical dataset contains approximately 30–40 slices, depending on the size of the breast. The time interval between the individual 3-D scans of the postcontrast sequence is approximately one minute. However, since most of the motion occurs immediately after the injection of the contrast agent, we have used only the first image of the postcontrast sequence.

To assess the registration quality in the patient datasets, we asked two clinical radiologists to assess the images visually

and to rank them according to their quality (where the lowest rank corresponds to the best quality). We compared no registration as well as the following three registration techniques: 1) rigid, 2) affine, and 3) the proposed nonrigid registration technique. For the nonrigid registration technique we used a control point spacing of 10 mm, since this has provided the best results in the volunteer experiments. The radiologists were presented with the pre-contrast images, the postcontrast images, and the corresponding difference images in a blinded fashion. The results of the ranking and significance tests for all pairwise multiple comparison procedures are summarized in Table II. In 94% of the cases, both radiologists ranked the nonrigid registration technique as the best technique. In the remaining 6% of the cases, there was very little motion between the pre- and postcontrast images so that all

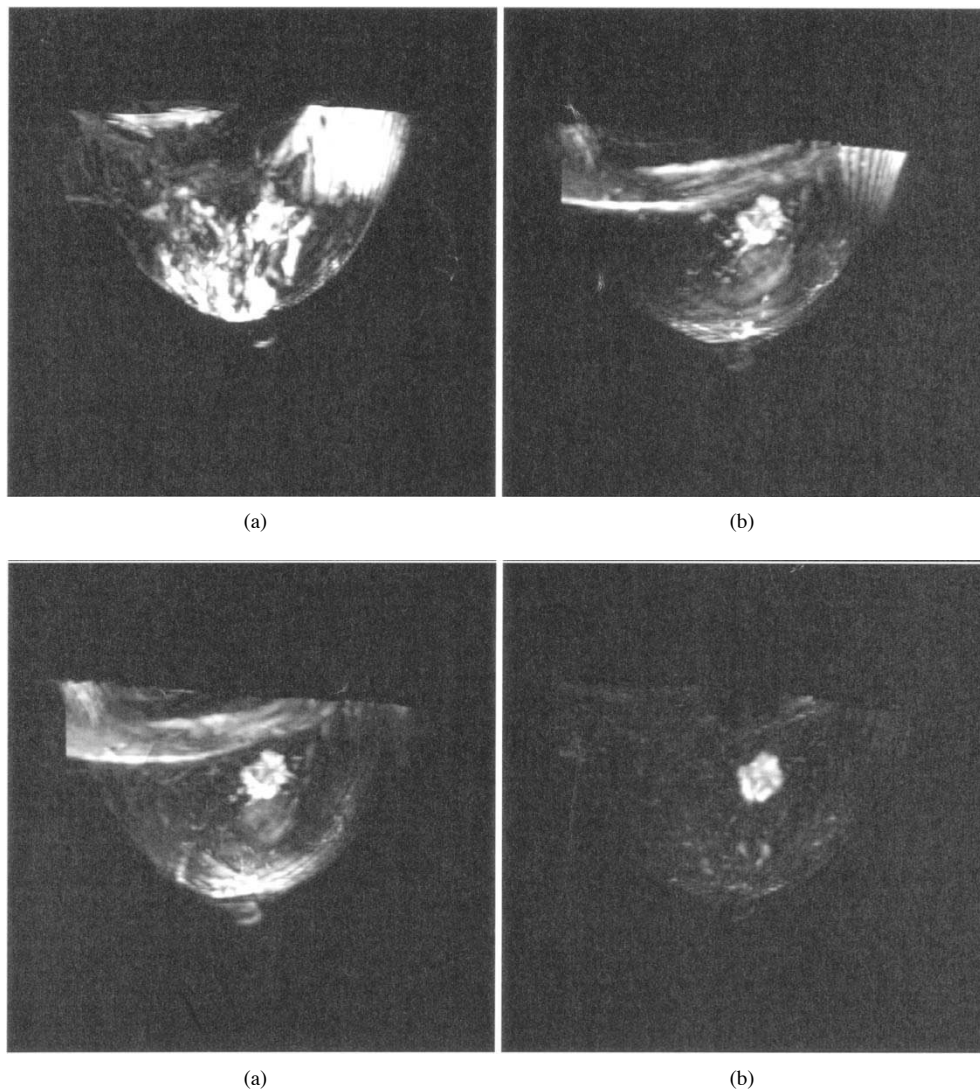


Fig. 8. A MIP of the difference images of the patient study in Fig. 6. (a) Without registration. (b) With rigid. (c) With affine. (d) With nonrigid registration. The tumor can be recognized after registration with all three techniques, but is most clearly visible in (d).

TABLE I
COMPARISON OF THE AVERAGE REGISTRATION ERROR OF THE VOLUNTEER STUDIES IN TERMS OF SQUARED SUM OF INTENSITY DIFFERENCES (SSD) AND CORRELATION COEFFICIENT (CC) FOR DIFFERENT TYPES OF TRANSFORMATION. THE SPLINE-BASED FFD HAS BEEN EVALUATED AT A CONTROL POINT SPACING OF 20, 15, AND 10 mm

Registration	SSD (mean)	SSD (variance)	CC
No registration	38.52	53.90	0.8978
Rigid	23.63	33.38	0.9604
Affine	21.38	29.84	0.9689
Affine + FFD (20mm)	14.35	23.43	0.9877
Affine + FFD (15mm)	13.28	20.91	0.9895
Affine + FFD (10mm)	12.53	19.25	0.9905

TABLE II
VISUAL ASSESSMENT AND RANKING OF THE REGISTRATION QUALITY IN THE PATIENT DATASETS BY TWO RADIOLOGISTS (WHERE THE LOWEST RANK CORRESPONDS TO THE BEST QUALITY)

Registration		Ranking		
A	B	A < B	A = B	A > B
Rigid	No registration	78 %	22 %	–
Affine	No registration	84 %	16 %	–
Affine + FFD	No registration	94 %	6 %	–
Affine	Rigid	13 %	78 %	9 %
Affine + FFD	Rigid	94 %	6 %	–
Affine + FFD	Affine	94 %	6 %	–

registration techniques ranked equally well. The table also shows that there is little difference in the ranking between the rigid and affine registration techniques.

An example of a pre- and postcontrast enhanced image of a patient data set without registration is shown in Fig. 6. The difference image shows a substantial amount of motion artifacts, due to considerable patient movement after the injection of the contrast agent. Fig. 7 shows the postcontrast enhanced image

and the corresponding difference images after rigid, affine, and nonrigid registration. The results demonstrate that all three registrations techniques lead to a significantly improved localization of the uptake of contrast agent, compared to the difference image in Fig. 6(c). The tumor is clearly visible in all three difference images, but is best defined in the difference image with nonrigid registration. This can be verified by inspecting a 3-D reconstruction of the difference image in the form of a maximum intensity projection (MIP). Fig. 8(a)

shows a MIP reconstruction, viewed from the positive z direction, without registration. The misregistration artifacts make a interpretation of the reconstruction very difficult. In the MIP reconstruction after rigid and affine registration in Fig. 8(b) and (c), the tumor conspicuity is improved but there is still a significant amount of misregistration artifacts visible, due to motion of the chest wall and skin. Finally, the MIP reconstruction after nonrigid registration in Fig. 8(d) shows a much improved definition of the tumor and a significant reduction of the misregistration artifacts. This confirms that the proposed nonrigid registration algorithm can eliminate misregistration artifacts while preserving enhancing regions.

IV. DISCUSSION

We have developed a fully automated algorithm for the nonrigid registration of 3-D breast MRI based on normalized mutual information. The algorithm uses a nonrigid transformation model to describe the motion of the breast in dynamic MR images. The proposed combination of affine transformations and spline-based FFD's provides a high degree of flexibility to model the motion of the breast. In contrast to physics-based deformation models [30], the algorithm makes no assumptions about the elastic properties of the breast tissue. Even though physics-based deformation models might seem an attractive alternative, for example to model additional constraints such as incompressibility, they are usually difficult to evaluate and verify. Moreover, the elastic properties of the breast tissues can vary significantly across patients and with age, which renders the application of such models difficult.

The experimental results have shown that the nonrigid registration of 3-D breast MRI can reduce motion artifacts between images significantly. The results have also demonstrated that in many cases rigid or affine registration techniques are not sufficient to correct motion in 3-D breast MRI. In some of the difference images a small amount of structure is visible, even after nonrigid registration. This may be caused by partial volume effects, which are more pronounced for acquisitions with poor resolution in the slice direction. In future screening studies a significant improvement of the image resolution is envisaged which will reduce partial volume effects further.

The registration of these images currently takes between 15–30 min of CPU time on a Sun Ultra 10 workstation, which makes routine application in a clinical environment possible. We have also demonstrated the applicability of the algorithm to the motion correction in contrast-enhanced MRI. However, further work is needed to assess and evaluate the impact of the algorithm for the detection and diagnosis of breast cancer, which is the topic of a forthcoming paper [31]. Future work will involve the application of the proposed registration algorithm to data from the MRC-supported U.K. study of MRI as a method of screening women at genetic risk of breast cancer.

ACKNOWLEDGMENT

The authors wish to thank Dr. E. Denton, Consultant Radiologist at King's Healthcare Trust, Dr. S. Rankin, Consultant Radiologist at Guy's and St. Thomas NHS Trust Hospital,

and Dr. A. Padhani, Consultant Radiologist at Royal Marsden Hospital, for their enthusiastic support. They would also like to thank Dr. H. Fischer, Siemens (Erlangen) for supplying acquisition sequences for the MRI measurements and the Advisory Group of the UK MR Breast Screening Study for the measurement protocol.

REFERENCES

- [1] "Incidence of and mortality from cancers of the lung, skin, breast and cervix," Office of Nat. Stat., London, U.K., Monitor MB1 96/2, 1996.
- [2] J. C. Weinreb and G. Newstead, "MR imaging of the breast," *Radiology*, vol. 196, pp. 593–610, 1995.
- [3] S. H. Heywang-Köbrunner and R. Beck, *Contrast-Enhanced MRI of the Breast*. Berlin, Germany: Springer-Verlag, 1995.
- [4] C. S. Zuo, A. P. Jiang, B. L. Buff, T. G. Mahon, and T. Z. Wong, "Automatic motion correction for breast MR imaging," *Radiology*, vol. 198, no. 3, pp. 903–906, 1996.
- [5] R. Kumar, J. C. Asmuth, K. Hanna, J. Bergen, C. Hulka, D. B. Kopans, R. Weisskoff, and R. Moore, "Application of 3D registration for detecting lesions in magnetic resonance breast scans," in *Proc. SPIE Medical Imaging 1996: Image Processing*, Newport Beach, CA, Feb. 1996, vol. 2710, pp. 646–656.
- [6] H. Fischer, M. Otte, C. Ehrhrt-Braun, S. Peschl, and J. Henning, "Local elastic motion correction in MR mammography," in *Proc. Int. Soc. Magnetic Resonance Medicine*, 1998, vol. 1, p. 725.
- [7] P. Hayton, M. Brady, L. Tarassenko, and N. Moore, "Analysis of dynamic MR breast images using a model of contrast enhancement," *Med. Image Anal.*, vol. 1, no. 3, pp. 207–224, 1997.
- [8] J. B. A. Maintz and M. A. Viergever, "A survey of medical image registration," *Med. Image Anal.*, vol. 2, no. 1, pp. 1–36, 1998.
- [9] C. Studholme, D. L. G. Hill, and D. J. Hawkes, "Multiresolution voxel similarity measures for MR-PET registration," in *Information Processing Medical Imaging: Proc. 14th Int. Conf. IPMI'95*, 1995, pp. 287–298.
- [10] A. Collignon, F. Maes, D. Delaere, D. Vandermeulen, P. Seutens, and G. Maral, "Automated multimodality image registration using information theory," in *Information Processing Medical Imaging: Proc. 14th Int. Conf. IPMI'95*, 1995, pp. 263–274.
- [11] P. Viola, "Alignment by maximization of mutual information," Ph.D. dissertation, Massachusetts Inst. Technol., Cambridge, MA, 1995.
- [12] C. Studholme, D. L. G. Hill, and D. J. Hawkes, "Automated 3-D registration of MR and CT images of the head," *Med. Image Anal.*, vol. 1, no. 2, pp. 163–175, 1996.
- [13] C. Studholme, D. L. G. Hill, and D. J. Hawkes, "Automated 3D registration of MR and PET brain images by multi-resolution optimization of voxel similarity measures," *Med. Phys.*, vol. 24, no. 1, pp. 25–35, 1997.
- [14] C. Studholme, D. L. G. Hill, and D. J. Hawkes, "An overlap invariant entropy measure of 3D medical image alignment," *Pattern Recognit.*, vol. 32, no. 1, pp. 71–86, 1998.
- [15] F. Maes, A. Collignon, D. Vandermeulen, G. Marechal, and R. Suetens, "Multimodality image registration by maximization of mutual information," *IEEE Trans. Med. Imag.*, vol. 16, pp. 187–198, Mar. 1997.
- [16] D. L. Collins, A. C. Evans, C. Holmes, and T. M. Peters, "Automatic 3D segmentation of neuro-anatomical structures from MRI," in *Information Processing Medical Imaging: Proc. 14th Int. Conf. IPMI'95*, 1995, pp. 139–152.
- [17] J. P. Thirion, "Image matching as a diffusion process: An analogy with Maxwell's demons," *Medical Image Analysis*, vol. 2, no. 3, pp. 243–260, 1998.
- [18] G. E. Christensen, M. I. Miller, J. L. Mars, and M. W. Vannier, "Automatic analysis of medical images using a deformable textbook," *Computer Assisted Radiology*. Berlin, Germany: Springer-Verlag, June 1995, pp. 146–151.
- [19] M. Bro-Nielsen, "Fast fluid registration of medical images," in *Proc. 4th International Conference Visualization in Biomedical Computing VBC'96*, 1996, pp. 267–276.
- [20] C. R. Meyer, J. L. Boes, B. Kim, P. H. Bland, K. R. Zasadny, P. V. Kison, K. Koral, K. A. Frey, and R. L. Wahl, "Demonstration of accuracy and clinical versatility of mutual information for automatic multimodality image fusion using affine and thin-plate spline warped geometric deformations," *Medical Image Analysis*, vol. 1, no. 3, pp. 195–207, 1997.
- [21] R. Szeliski and S. Lavallée, "Matching 3-D anatomical surfaces with nonrigid deformations using octree-splines," in *IEEE Workshop on Biomedical Image Analysis*, 1994, pp. 144–153.

- [22] S. Lee, G. Wolberg, K.-Y. Chwa, and S. Y. Shin, "Image metamorphosis with scattered feature constraints," *IEEE Trans. Visualization Comput. Graph.*, vol. 2, pp. 337–354, Oct. 1996.
- [23] S. Lee, G. Wolberg, and S. Y. Shin, "Scattered data interpolation with multilevel B-splines," *IEEE Trans. Visualization Comput. Graph.*, vol. 3, pp. 228–244, July 1997.
- [24] E. Bardinet, L. D. Cohen, and N. Ayache, "Tracking and motion analysis of the left ventricle with deformable superquadrics," *Med. Image Anal.*, vol. 1, no. 2, pp. 129–149, 1996.
- [25] F. L. Bookstein, "Principal warps: Thin-plate splines and the decomposition of deformations," *IEEE Trans. Pattern Anal. Machine Intell.*, vol. 11, pp. 567–585, June 1989.
- [26] M. H. Davis, A. Khotanzad, D. P. Flamig, and S. E. Harms, "A physics-based coordinate transformation for 3-D image matching," *IEEE Trans. Med. Imag.*, vol. 16, no. 3, pp. 317–328, May 1997.
- [27] D. R. Forshey and R. H. Bartels, "Hierarchical B-spline refinement," *ACM Trans. Comput. Graph.*, vol. 22, no. 4, pp. 205–212, 1988.
- [28] G. Wahba, "Spline models for observational data," *Soc. Industr. Applied Math.*, 1990.
- [29] J. B. West, J. M. Fitzpatrick, M. Y. Wang, B. M. Dawant, C. R. Maurer, Jr., R. M. Kessler, R. J. Maciunas, C. Barillot, D. Lemoine, A. Collignon, F. Maes, P. Suetens, D. Vandermeulen, P. A. van den Elsen, S. Napel, T. S. Sumanaweera, B. Harkness, P. F. Hemler, D. L. G. Hill, D. J. Hawkes, C. Studholme, J. B. A. Maintz, M. A. Viergever, G. Malandain, X. Pennec, M. E. Noz, G. Q. Maguire, Jr., M. Pollack, C. A. Pelizzari, R. A. Robb, D. Hanson, and R. P. Woods, "Comparison and evaluation of retrospective intermodality image registration techniques," *J. Comput. Assisted Tomogr.*, vol. 21, pp. 554–566, 1997.
- [30] P. J. Edwards, D. L. G. Hill, J. A. Little, and D. J. Hawkes, "A three-component deformation model for image-guided surgery," *Med. Image Anal.*, vol. 2, no. 4, pp. 355–367, 1998.
- [31] E. R. E. Denton, L. I. Sonoda, D. Rueckert, S. C. Rankin, C. Hayes, M. Leach, D. L. G. Hill, and D. J. Hawkes, "Comparison and evaluation of rigid and nonrigid registration of breast MR images," *J. Comput. Assisted Tomogr.*, 1999, to be published.